

Joseph A. Santanello, Jr.<sup>\*1,2</sup>, Christa D. Peters-Lidard<sup>2</sup>, and S. V. Kumar<sup>2,3</sup>  
<sup>1</sup>ESSIC/UMCP, <sup>2</sup>NASA-GSFC Hydrological Sciences Branch, <sup>3</sup>GEST/UMBC

## 1. INTRODUCTION

Land-atmosphere (L-A) interactions and coupling remain weak links in current observational and modeling approaches to understanding and predicting the Earth-Atmosphere system. The degree to which the land impacts the atmosphere (and vice-versa) is difficult to quantify given the disparate resolutions and complexities of land surface and atmospheric models and lack of comprehensive observations at the process level (Betts et al. 1996; Angevine 1999; Entekhabi et al. 1999; Cheng and Steenburgh 2005; Gu et al. 2006). However, the convective planetary boundary layer (PBL) serves as a short-term memory of land surface processes (through the integration of regional surface fluxes on diurnal scales), and therefore is diagnostic of the surface energy balance. Further, the mixed-layer and land surface equilibrium reached each day describes the degree of coupling and the impact of feedbacks within the L-A system (Pan and Mahrt 1987; Stull 1988; Diak 1990; Garratt 1992; Dolman et al. 1997; Peters-Lidard and Davis 2000; Cleugh et al. 2003; Betts and Viterbo 2005). As such, knowledge of temperature and moisture evolution in the PBL can be instrumental in estimating surface fluxes and properties across regional scales as well as quantifying and improving L-A representations in coupled models.

While recent progress has been made in identifying individual L-A processes and feedback loops for a particular location or model (Margulis and Entekhabi 2001; Barros and Hwu 2002; Ek and Holtslag 2004; Santanello et al. 2005, 2007), a comprehensive approach to diagnosing the full nature of L-A coupling that can be applied to models and evaluated against observations has yet to be developed. The need for such a framework will only become more critical as advances in remote sensing continue to provide a wealth of information on the land surface and PBL that can be incorporated into L-A studies and models (e.g. data assimilation), but must be done so properly.

A relatively simple but untested approach to quantifying heat and moisture budgets in the PBL has been presented by Betts (1992) that is based upon a vector representation of the diurnal change in temperature and humidity. Application of this 'mixing diagram' theory to models and observations would offer the ability to perform a robust evaluation of L-A interactions with minimal inputs due to the integrative nature of the mixed layer on diurnal time scales. Ideally, this approach should be tested using a coupled,

high-resolution, mesoscale model with flexible land surface and PBL schemes, thereby allowing the variation in L-A coupling among different formulations versus that observed to be evaluated.

With these issues in mind, this paper defines a methodology to quantify local L-A coupling and the various components and feedbacks therein. Section 2 presents background on the mixing diagram approach that is adopted and extended in this study. The coupled regional model, land surface models, and PBL schemes used in the experiments are highlighted in Section 3 along with detailed information on the sites, case studies, and associated observations. Results and analyses of the mixing diagram approach applied to these experiments are presented in Section 4. Finally, Section 5 discusses the overall applicability and limitations of the methodology, and an initiative for a community effort to participate in local L-A coupling experiments.

## 2. BACKGROUND AND METHODOLOGY

### 2.1 Motivation for Studying L-A Coupling

The need for improved understanding, estimation, and prediction of L-A interactions and feedbacks has been growing significantly over the last decade (Jacobs and DeBruin 1992; Kim and Entekhabi 1998; Liu et al. 2005; Medeiros et al. 2005; Dirmeyer et al. 2005). During this time, offline (uncoupled) land surface models (LSMs) have grown in complexity and diversity, while the ability to evaluate these models offline, such as during the Project for Intercomparison of Land-surface Parameterization Schemes (PILPS) experiments (Henderson-Sellers et al. 1996), has come into question due to the omission of L-A feedbacks. At the same time, LSMs coupled to atmospheric models are often highly tuned to each other without regard for the degree and accuracy of coupling between the L-A schemes or the impact of feedbacks. In both instances, our ability to diagnose and quantify these interactions is lacking, and needs to be improved by evaluating the best available PBL and land surface data in the context of the equilibrium established between the two through their interactions and feedbacks, and how this compares to what is simulated in our models.

Currently, L-A coupling is being addressed through organized, community-wide studies focusing on large scale offline (Global Soil Wetness Project (GSWP; REF), large scale coupled (Global Land Atmosphere Coupling Experiment (GLACE); Koster et al. 2002), and local scale offline (PILPS) models. To date, however, an organized effort to study the critical processes involved in *local land-atmosphere coupling* (hereafter referred to as 'LoCo') has yet to come to fruition.

---

\*Corresponding author address: Joseph A. Santanello, Jr., Room 8, Bldg. 22, NASA-GSFC Code 614.3, Greenbelt, MD 20771; [Joseph.A.Santanello@nasa.gov](mailto:Joseph.A.Santanello@nasa.gov)

There have been a host of studies focused on a variety of individual L-A processes and feedbacks that call for further study of LoCo in a comprehensive and quantitative manner. For example, Cheng and Steenburgh (2005) show that errors in sensible weather forecasts from two leading mesoscale models are severely limited by insufficient parameterization of LoCo processes and the need for a more concerted effort in this regard. Similarly, Gu et al. (2006) call for improved representation of LoCo in models while examining the impacts of soil moisture on energy balance partitioning and corresponding feedbacks from a microclimate perspective. Betts (2000) and Betts and Viterbo (2005), while evaluating global model reanalysis data, show that the L-A coupling is critical in such large-scale models, but the critical processes and relationships that determine model evolution and equilibrium lie on the local scale and are lacking sufficient understanding and representation in models of all scales.

Inherent in the ability to accurately simulate L-A interactions in coupled models is the engineering of the coupling itself in terms of model design and variable passing from land surface to surface layer and PBL schemes, and vice-versa. As shown by Polcher et al. (1998), Molod et al. (2004), and Chen et al. (1997), the specific design of coupling remains a largely model-dependent decision based on ease of implementation, when in practice the optimal coupling structure should be determined by which results in the most accurate representation of the L-A processes. Given the current lack of understanding and observations of these processes, this most accurate structure is therefore unknown and/or untested before models are implemented.

### **b. Mixing Diagram Approach**

It is apparent from these studies that in order for a robust methodology to diagnose coupling to be effective and useful to the community, it must be comprehensive and integrative of L-A processes and feedbacks; while at the same time able to be implemented using easily observed and understood properties of the system.

An approach that may satisfy these requirements for local and diurnal time scales is the concept of vector representation of heat and moisture (energy) budgets, as introduced by Betts (1984, 1992) in the form of 'mixing diagrams'. This conservative variable approach relates the diurnal evolution of specific humidity ( $q$ ) and potential temperature ( $\theta$ ) to the land surface and mixed layer energy balance and, in effect, the diurnal equilibrium established by L-A interactions. The daytime variability of  $\theta$  and  $q$  is sensitive to and, in fact, integrative of the dominant processes involved in LoCo, and when plotted in energy space ( $Lq$  vs.  $C_p\theta$ ) can be used to quantify these processes.

Figure 1 shows an example of a mixing diagram for the 12-hour change in  $Lq$  and  $C_p\theta$  as simulated by a coupled mesoscale model during June 2002 at a point in Oklahoma. For a full derivation and discussion of this theory we refer the reader to Betts (1992). The change from 12Z to 00Z is fully described by vector components

that represent the fluxes of heat and moisture from the land surface and the top of the PBL (entrainment). These two vector components ( $\mathbf{V}_{sfc}$  and  $\mathbf{V}_{ent}$ ) have a slope equal to the Bowen ratio of the surface and entrainment fluxes ( $\beta_{sfc}$ ,  $\beta_{ent}$ ). Their magnitudes, in terms of  $C_p\Delta\theta$  and  $L\Delta q$ , are proportional to the fluxes of heat ( $H$ ) and moisture ( $LE$ ) of each. For example, the magnitude of the surface vector component in the y-direction (heat) is as follows,

$$C_p\Delta\theta_{sfc} = \frac{\overline{H_{sfc}} \cdot \Delta t}{\rho_m \cdot PBLH} \quad (1)$$

which can be calculated from the mean sensible heat flux ( $H_{sfc}$ ) over the time interval ( $\Delta t$ ), the density in the mixed layer ( $\rho_m$ ), and the height of the mixed layer ( $PBLH$ ). Once the surface vector is known, the entrainment flux ( $H_{ent}$ ) can then be backed out as the vector that connects  $\mathbf{V}_{sfc}$  to the final values of  $C_p\theta$  and  $Lq$  at 00Z. The analogous formulation holds for the flux of moisture at the surface (i.e. evapotranspiration;  $LE_{sfc}$ ) and top of the PBL (i.e. dry air entrainment  $LE_{ent}$ ).

Having derived the slope ( $\beta_{ent}$ ) and magnitude ( $C_p\Delta\theta_{ent}$ ) of  $\mathbf{V}_{ent}$ , the entrainment ratio ( $A_R = H_{ent}/H_{sfc}$ ), defined as the proportion of heat input to the PBL from entrainment to that of the surface, can be easily quantified. Typically,  $A_R$  is specified as a constant in models but there has been little consensus as to what the value should be based on different empirical studies (REFs). The mixing diagram approach is extremely valuable in this regard, considering that difficulties in observing and measuring fluxes at the top of the PBL greatly limit efforts to close energy budgets in the PBL (e.g., Peters-Lidard and Davis 2000; Santanello et al. 2005). Similarly, the entrainment of moisture (typically negative due to drier air in the free atmosphere) is easily quantified using this methodology. Therefore we find it useful to define separately a heat and moisture entrainment ratio ( $A_h$  and  $A_{le}$ , respectively) when discussing the components of the energy budgets derived from mixing diagrams.

Betts (1992), Betts and Ball (1995) and Betts et al. (1996) provide the foundation for this approach and apply it to empirical data from a short-term field experiment. They show, qualitatively, how the diurnal evolution of  $q$  and  $\theta$  strongly reflects conditions and processes at the land surface (soil moisture, evaporation) and the top of the PBL (entrainment) as the theory suggests. For example, Figure 2 shows a mixing diagram for three days based on composites of different soil moisture conditions from 28 days of data. Although the vector and flux components are not calculated here, a visual examination of these curves indicate the different nature of L-A interactions for dry, intermediate, and wet soils. In particular, the entrainment (represented by mid-late day drying of the mixed-layer and lower  $q$ ) is largest for dry surface conditions which lead to increased buoyancy, mixing, and PBL growth. In contrast, the wet surface evaporates freely throughout the day, moistening the shallower PBL, with a negligible impact of entrainment.

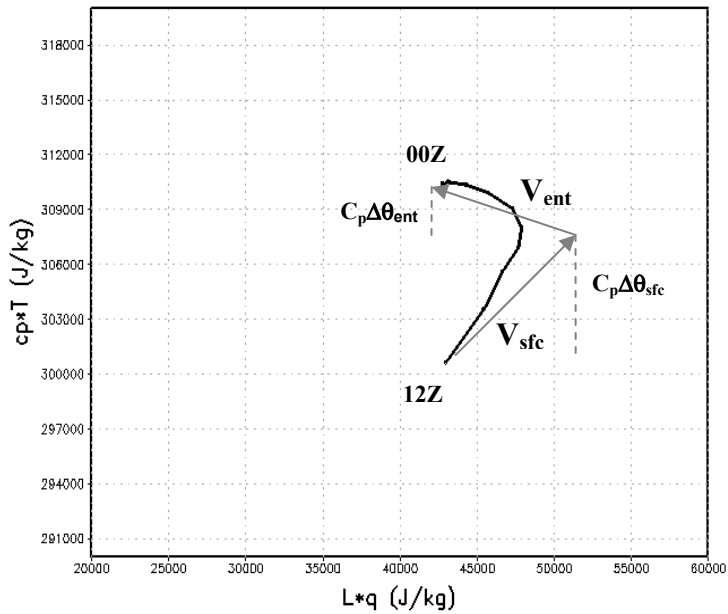


**Figure 1:** Diurnal evolution (12-00Z; solid red line) of 2m-potential temperature ( $C_p \theta$ ) vs. 2m-specific humidity ( $Lq$ ) on 12 June 2002 simulated by LIS-WRF using the Noah LSM with the YSU PBL scheme during the IHOP-02 experiment in the SGP. The annotations on the plots depict the vector component contributions of surface and entrainment fluxes.

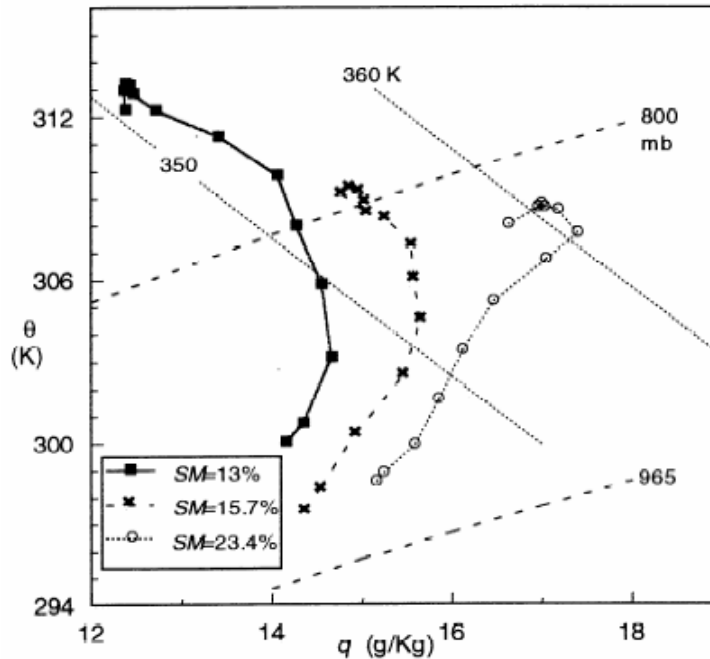


**Figure 2:** Diurnal evolution (12-00Z) of 2m-potential temperature ( $\theta$ ) vs. 2m-specific humidity ( $q$ ) for 28 days from July and August 1987 during the FIFE campaign, composited by soil moisture. [Figure reproduced from Betts et al. 1996]

By quantifying these processes using the theory outlined above, the exact nature of L-A interactions and critical feedbacks (such as those identified by Santanello et al. 2007) can be evaluated in coupled models and compared against observations. The relatively few input requirements are standard output for most models, and in essence the only temporal resolution required is the initial (12Z) and final (00Z) values of  $q$  and  $\theta$  in order to identify the integrative processes and feedbacks controlling LoCo.

### 3. MODEL AND SITE SPECIFICATION

#### 3.1 WRF and LIS-WRF

The Advanced Research version of the Weather Research and Forecasting (WRF-ARW) model (Michalakes et al. 2001) is a state of the art mesoscale numerical weather prediction system designated as the community model for atmospheric research and operational prediction, and is ideal for regional simulations on the order of 1-7 days. The model has a Eulerian mass dynamical core and includes a wide array of radiation, microphysics, and PBL options as well as 2-way nesting and variational data assimilation capabilities.

To serve as a testbed for LoCo diagnostics, WRF-ARW (Version 2.1.2) has been coupled to NASA's Land Information System (LIS; Version 4.2) by Kumar et al. (2008). LIS consists of a suite of LSMs and provides a flexible and high-resolution representation of land surface physics and states which are directly coupled to the atmosphere (hereafter referred to as LIS-WRF). The advantages of coupling LIS to WRF-ARW include the ability to spin-up land surface conditions on a common grid from which to initialize the regional model, flexible and high-resolution soil and vegetation representation, additional choices of LSMs that will continue to grow, and various plug-in options such as land data assimilation and parameter estimation. LIS-WRF has been tested extensively thus far over the U.S. Southern Great Plains (SGP), Florida, the Gulf of Mexico, and Korea, and recently has been upgraded to include LIS Version 5.0 with WRF-ARW Version 2.2.

The LSMs employed in LIS for this study are the Noah LSM (Noah; Ek et al. 2003), and the Community Land Model Version 2.0 (CLM; Dai et al. 2003). Both models dynamically predict water and energy fluxes and states at the land surface, but vary in specific parameterizations and representation of soil and vegetation properties and physics. The Noah model employed in this study is Version 2.7.1 and is identical to the version of Noah packaged in the original version of WRF-ARW, whereas CLM is unique to LIS-WRF.

There are three options for PBL schemes in WRF-ARW, all of which are employed in this study using LIS-WRF. The Medium-Range Forecast (MRF; Hong and Pan 1996) scheme is based on non-local-K theory. (Troen and Mahrt 1986) mixing in the convective PBL, The Yonsei University (YSU; Hong et al. 2006) scheme, based on the MRF, is also a non-local K theory implementation, but includes explicit treatment of

entrainment and counter gradient fluxes. Finally, the Mellor-Yamada-Janjic (MYJ; Janjic 2001) scheme is the most complex PBL scheme, and employs nonsingular level 2.5 turbulent kinetic energy (TKE) closure (from Mellor and Yamada 1982) with local-K vertical mixing.

#### 3.2 LIS-WRF Experimental Design

To address LoCo under the LIS-WRF framework, simulations were performed using the Noah and CLM LSMs with the MRF, YSU, and MYJ PBLs, for a total of 6 different combinations of L-A coupling (the remainder of the LIS-WRF setup is identical for each). The results of each experiment is then evaluated using the mixing diagram approach described above, where the processes and feedbacks generated by each LSM-PBL pair are quantified over the course of the day for different locations and conditions and compared with observations.

As shown by Koster et al. (2005) and others, the SGP region is a hotspot for L-A coupling in terms of the strength of interactions and feedbacks. Because of this, and the wealth and record of observational data from the Atmospheric and Radiation Measurement (ARM) testbed located in the region (ARM-SGP), numerous intensive field campaigns have been conducted in the region that have augmented the instrument and data quality even further. For this study, simulations have been performed for two of these campaigns: a) the International H<sub>2</sub>O Project in June 2002 (IHOP-02; Weckworth et al. 2004) and b) the Cooperative Atmosphere-Surface Exchange Study (CASES-99; Poulos et al. 2002) in October 1999. During IHOP-02, we chose to focus on 36-hour simulations centered on June 6 and June 12, as they represent a clear-sky 'golden' day, and an unstable day with spatially heterogeneous convection, respectively. CASES-99 was chosen because it was recently used as a focused experiment by the GABLS community of PBL modelers. The interest of LoCo in GABLS and vice-versa made this a desirable case, and we chose to perform 72-hour simulations covering 23-26 October 1999 that consisted of relatively benign daytime conditions over the SGP with variably turbulent nocturnal PBLs.

For each experiment, LIS-Noah and LIS-CLM were run offline (uncoupled) for the 2.5 year period prior to the start time of IHOP-02 and CASES-99 to create equilibrated, or spun-up, land surface states for initialization of LIS-WRF. Overall, conditions in the ARM-SGP region range from highly vegetated and moist in the east to increasingly bare and drier soils in the west.

#### 3.3 ARM-SGP Observations

The ARM-SGP site provides surface flux, meteorological, and hydrological observations along with atmospheric profiles for a network of sites in and near the winter wheat belts of Oklahoma and Kansas.

Radiosondes are launched daily at approximately 1130, 1430, 1730, and 2030 UTC (6:30am 9:30am, 12:30pm, and 3:30pm local time) at the SGP central

facility at Lamont, OK (CF). For this work, radiosonde measurements of temperature, dewpoint, and pressure were converted to profiles of  $\theta$  and  $q$  at  $\sim 10$  m vertical resolution using standard thermodynamic relationships, from which estimates of the height of the PBL (inversion) were derived.

The ARM-SGP site employs both Bowen ratio (EBBR) instruments at CF as well as numerous extended facilities throughout Kansas and Oklahoma. These data include 30-minute average fluxes of net radiation, sensible, latent, and soil heat, along with co-located surface radiant temperature, 2-m air temperature, mixing ratio, and wind measurements from micrometeorological instrumentation. Soil moisture measurements were also collected at the CF and extended facilities with 5 sampling locations distributed across a 10-meter area at each of the sites.

## 4. RESULTS

The following sections present mixing diagrams generated from LIS-WRF simulations of the IHOP-02 and CASES-99 experiments. As described above, generation of these plots and derived metrics requires only the diurnal evolution of  $\theta$  and  $q$ , average  $H_{sfc}$ , and maximum  $PBLH$ , all which are routinely output from LIS-WRF and observed at ARM-SGP.

### 4.1 Mixing Diagrams

#### 4.1.1 IHOP-02 across moisture regimes

The principal controls on the fluxes of heat and moisture from the surface reside in the degree of soil moisture and vegetation cover. During spring and summer over the ARM-SGP region, there is high spatial variability in each of these that we can use to examine LoCo across a range of conditions. Figure 3 shows mixing diagrams from LIS-WRF-Noah and LIS-WRF-CLM simulations on 12 June 2002 for a location with dry soil moisture conditions ( $0.08 \text{ m}^3 \text{ m}^{-3}$ ) in the western part of the domain. The impacts of coupling the three PBLs to each LSM can be seen in the differences in the evolution of  $\theta$  and  $q$ .

Qualitatively, the overall shape of the curves indicates little evaporation from the surface and significant dry air entrainment into the PBL. The metrics derived through these diagrams are also plotted and confirm a high  $\beta_{sfc}$  and surface heating, while the entrainment flux is primarily that of dry air ( $\beta_{ent} \sim -0.30$ ) that causes the PBL to dry out and grow rapidly during the mid-late afternoon. The large magnitudes of  $A_h$  and  $A_{le}$  also confirm that the entrainment fluxes of heat and moisture dominated over the fluxes from the surface, another indicator of rapid and deep PBL growth over a dry surface (the values for maximum  $PBLH$  are each well over 3 km). In fact, this type of mixing diagram 'signature' is indicative of an entrainment feedback loop that promotes deep PBL growth, drying of the PBL, and desiccation of the surface leading to drought if

persistent over time given consistent synoptic conditions (as described in Santanello et al. 2007).

The subtle but significant differences within and between the two diagrams are reflective of differences in PBL-LSM coupling and can be identified using the derived metrics. For the Noah LSM (Fig. 3a), the equilibrium created with all three PBLs is similar, but the YSU scheme shows the largest entrainment of heat and moisture and the MYJ scheme the least. This is confirmed in the vertical profile data (not shown), where the YSU has an extremely deep PBL (4.7 km) versus that of the MYJ (2.4 km), with the MRF scheme in between (3.7 km).

For the CLM simulations (Fig. 3b), there is a significant difference in the coupling established by the 3 PBLs, with the MYJ deviating from the YSU and MRF schemes (and the Noah LSM). The surface fluxes are similar for each with very little evaporation, but the MYJ entrains air that is slightly warmer and moister than the YSU and MRF schemes. As a result, there is more warming of the PBL throughout the day for the MYJ scheme, but also significant drying which again indicates rapid and deep PBL growth. Profiles indicate similar  $PBLH$  values to the Noah simulations for all three PBLs. Once again, the YSU shows the largest heat and moisture entrainment fluxes, but all three are reflective of a desiccated, largely bare soil, surface and significant entrainment feedback into the PBL.

Figure 4 presents mixing diagrams for more intermediate soil moisture conditions ( $0.18 \text{ m}^3 \text{ m}^{-3}$ ) in the ARM-SGP region as simulated by LIS-WRF using the Noah and CLM LSMs. For all PBL-LSM combinations shown in Figs. 4a and 4b, there is a significantly different signature of  $\theta$  and  $q$  evolution than for dry soils. Most significantly, there is little diurnal variability in specific humidity and a lower dynamic range in  $\theta$ , which is expected due to L-A interactions over a more moist and vegetated surface.

As described by the metrics, more energy at the surface goes to evaporation ( $\beta_{sfc}$ ), particularly for the Noah model, which lowers the amount of surface heating and flux of heat into the PBL. As a consequence, there is less buoyancy and slower PBL growth, reflected in the much lower proportion of dry air entrainment ( $A_{le}$ ) than for dry soils. The damped evolution of  $q$  is a result of the magnitudes of surface evaporation relative to that of dry air entrainment, which nearly balance for this location. In this case, there is near zero flux of heat into the PBL from entrainment, and CLM actually indicates some cooler air mixing through the inversion. Maximum  $PBLH$  was approximately 1.4 km for the MRF and MYJ simulations, while the YSU PBL was slightly higher ( $\sim 1.7$  km; not unexpected given the difference in physics and explicit entrainment treatment in the YSU scheme). As for the dry soil case, the PBL evolution and structure is more significantly impacted by the specific PBL scheme employed than by the choice of LSM.

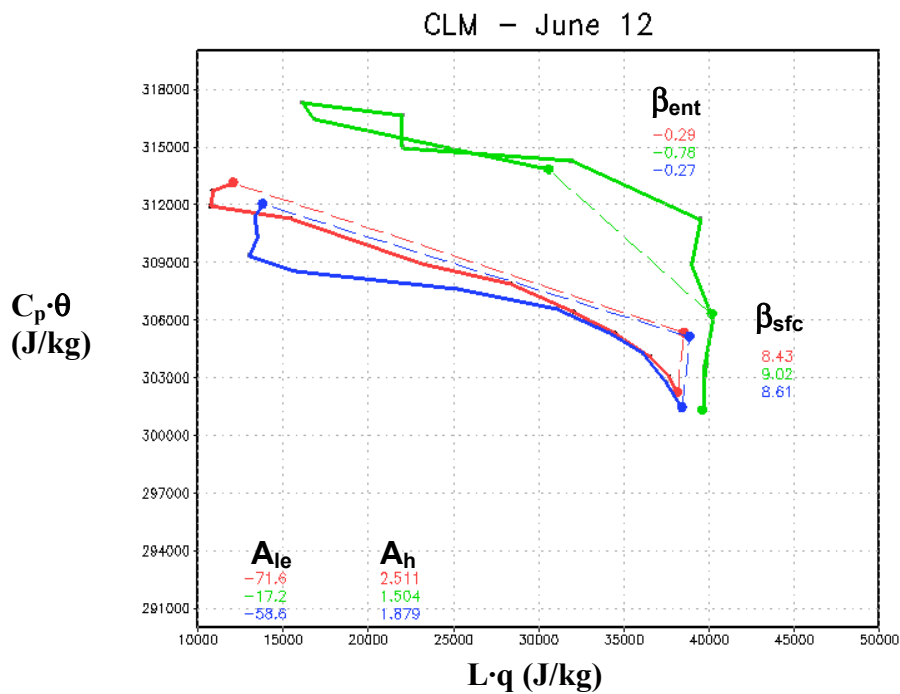
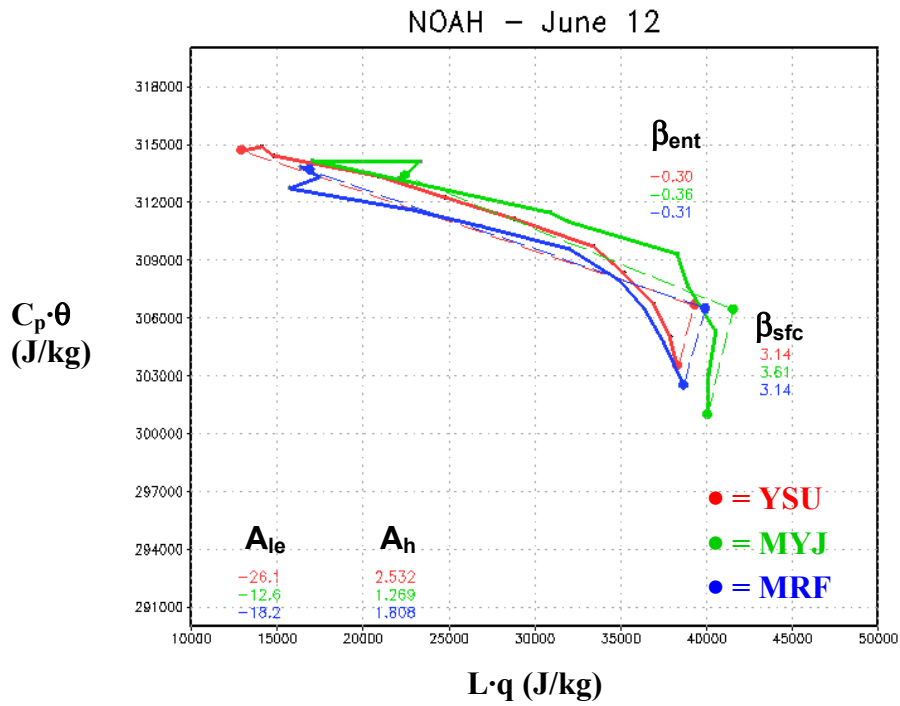


**Figure 3:** Diurnal co-evolution (12-00Z) of 2m-specific humidity ( $Lq$ ) and 2m-potential temperature ( $C_p\theta$ ) on 12 June 2002 as simulated by LIS-WRF during dry soil moisture conditions ( $0.08 \text{ m}^3 \text{ m}^{-3}$ ) in the Southern Great Plains using the a) Noah and b) CLM land surface models with the YSU (red solid), and MYJ (green solid), and MRF (blue solid) PBL schemes. Also shown are the surface ( $\mathbf{V}_{sfc}$ ) and entrainment ( $\mathbf{V}_{ent}$ ) vectors (dashed lines), surface ( $\beta_{sfc}$ ) and entrainment ( $\beta_{ent}$ ) Bowen ratio values, and heat ( $A_h$ ) and moisture ( $A_{ie}$ ) entrainment ratios.

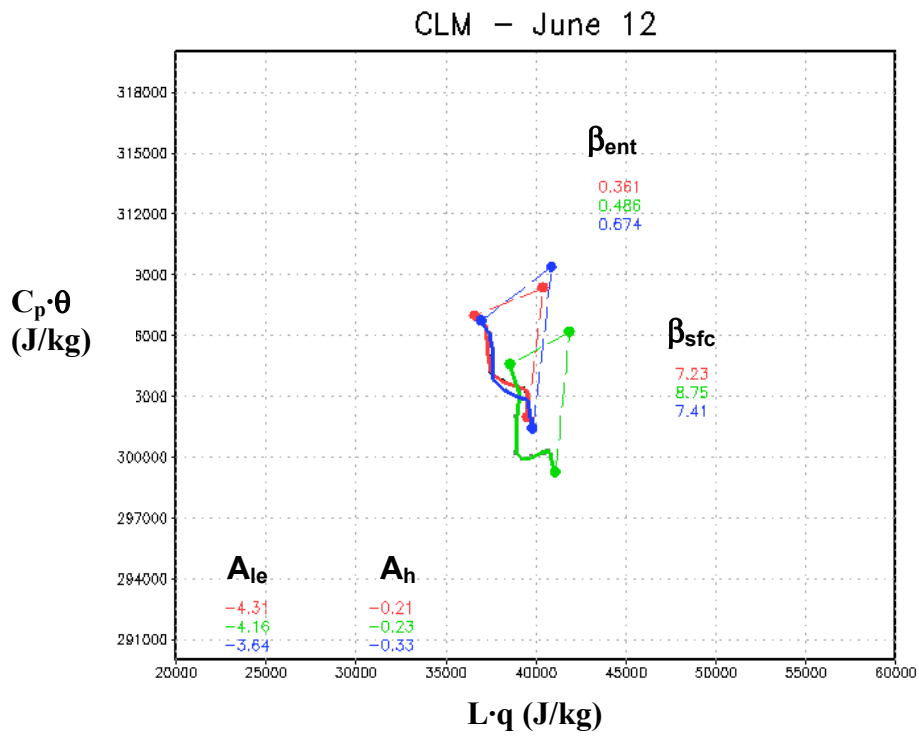
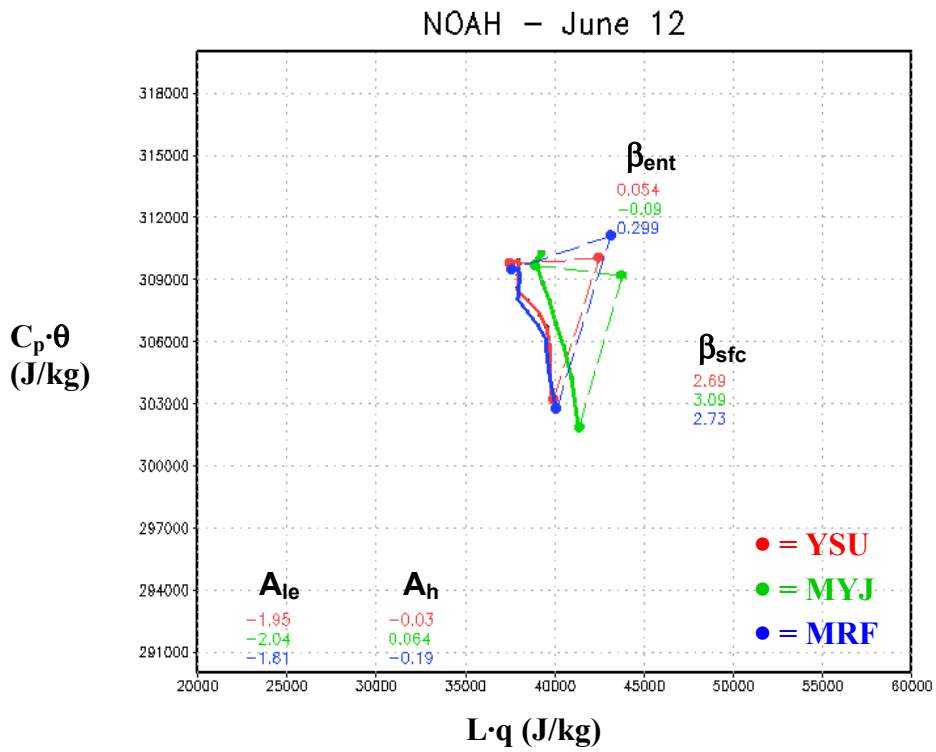


Figure 4: Same as Figure 3, but for intermediate soil moisture conditions ( $0.18 \text{ m}^3 \text{ m}^{-3}$ ).

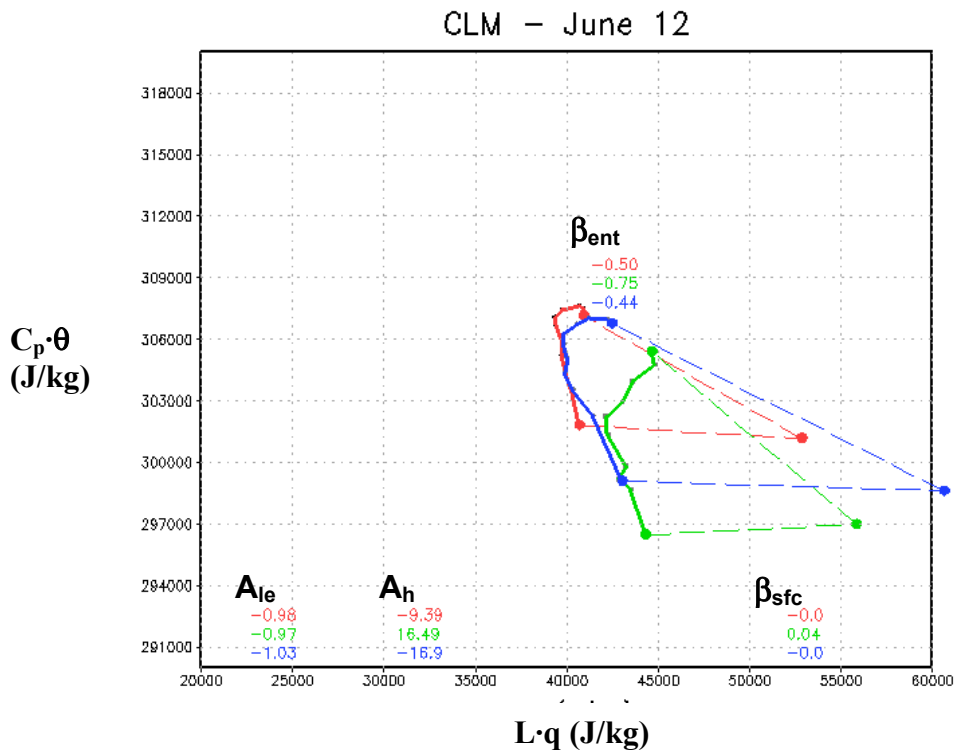
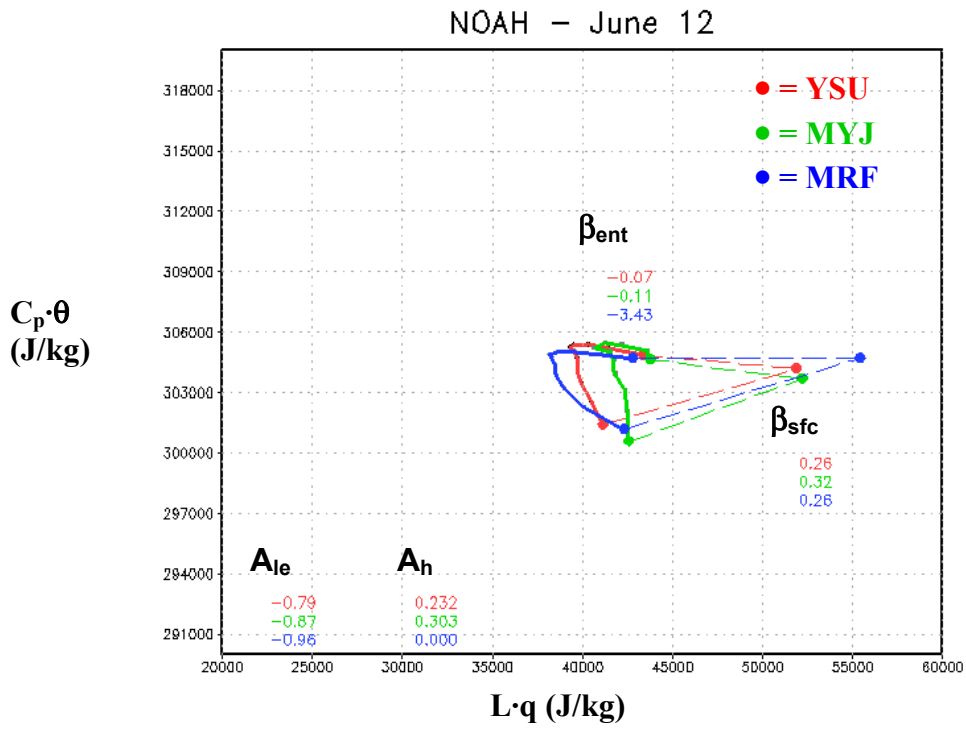


Figure 5: Same as Figure 3, but for wet soil moisture conditions ( $0.32 \text{ m}^3 \text{ m}^{-3}$ ).

Figure 5 shows mixing diagrams for wet soil conditions ( $0.32 \text{ m}^3 \text{ m}^{-3}$ ) in the eastern portion of the domain, which is also more heavily vegetated. What is immediately evident for the Noah simulations in Fig. 5a is the small range in both  $\theta$  and  $q$  and the dominance of the moisture fluxes controlled by a nearly freely evaporating surface (low  $\beta_{\text{sfc}}$ ) and dry air entrainment (low  $\beta_{\text{ent}}$ ). The pattern from each of the three PBL schemes is similar, and there is very little surface heating and PBL growth ( $PBLH \sim 0.8 \text{ km}$ ) for this location as well. The turn towards higher  $q$  in the late afternoon is a significant feature of this mixing diagram signature (and counter to the dry air entrainment flux) that will be discussed later.

The CLM simulations (Fig. 5b) produce a different heat and moisture evolution than Noah at this location for all three PBLs. While the surface energy balance is similar and surface evaporation is dominant (near zero  $\beta_{\text{sfc}}$  due to an initial condition that is slightly wetter than Noah), there is more entrainment of heat into the PBL than for Noah (higher  $\beta_{\text{ent}}$ ), allowing for a more significant rise in  $\theta$  throughout the day. This is a result of more significant PBL growth in the CLM simulations ( $PBLH \sim 1.5 \text{ km}$ ). For all three simulations over the wet surface,  $A_{1e}$  is approximately equal to  $-1.0$  which indicates the near balance of evaporation with entrainment. The differences in the coupling created by Noah with CLM lie in the amount of heat entrained and the depth of the PBL.

#### 4.1.2 IHOP-02 and CASES-99 with observations

Overall, Figs. 3-5 demonstrate the power and relative ease of using mixing diagrams to portray and quantify complex L-A interactions and feedbacks and their sensitivities to different L-A coupling and surface conditions. These cases suggest that the sensitivity to PBL or LSM choice depends on the specific surface and atmospheric conditions, and significant sensitivities are evident in each. This approach can now be supplemented with observations in the same manner in order to evaluate these simulations in the context of the impacts of their different L-A coupling. It is also important to note that it is not the goal of this study to perform an intensive evaluation of the PBL and LSM schemes employed here, but rather to use these experiments to present a framework to further evaluate and understand any coupled modeling system.

Mixing diagrams from LIS-WRF simulations are presented in Fig. 6 with observations made at the ARM-SGP Central Facility (CF; E13) on June 6 2002. The results of the Noah simulations with all three PBLs do an excellent job of reproducing the observed evolution of  $\theta$  and  $q$ . In contrast, the CLM tends to diverge appreciably from the observations and in opposing directions depending on the PBL scheme. Once again, the YSU and MRF schemes results are similar for each LSM.

A closer look at the metrics shows that although the Noah model simulates a slightly higher  $\beta_{\text{sfc}}$  than observed, the resultant PBL evolution and mixing produces an accurate  $\theta$  and  $q$  equilibrium. In addition,

PBL heights generated by the YSU, MYJ, and MRF schemes (1.4, 1.6, and 1.3 km, respectively) are close to observed (1.5 km). The coupling of CLM with the 3 PBLs, on the other hand, results in 2 simulations (YSU and MRF) that tend to dry out immediately and overestimate PBL growth ( $\sim 1.9 \text{ km}$ ) and dry air entrainment, and 1 simulation (MYJ) that shows an initial moistening of the mixed layer (that incidentally shows similarities to observations) that greatly limits PBL growth (1.1 km) and delays the impact of entrainment.

Another potentially informative feature of these diagrams is that the variability in the diurnal range of  $\theta$  and  $q$  is immediately evident in the starting and end points. In some simulations, a slightly warmer/moister starting point may be significant enough to support a vastly different set of L-A interactions and PBL evolution (e.g. Fig. 6b), while in other cases the range of each and dynamics remain similar.

The CASES-99 experiment occurred during a rather uniform land surface and synoptic condition in mid-fall. However, the 72-hour LIS-WRF integrations performed for this study allow us to examine the impact of different PBL-LSM couplings on multi-day simulations. Figure 7 presents mixing diagrams with observations at CF from the third and final day (October 25) of this period. It is apparent that the overall evolution and slope of  $\theta$  and  $q$  are similar for all simulations and close to observations. However, the Noah simulations capture the absolute diurnal range more closely than those with CLM, which are offset from initial time and suffer throughout the remainder of the day despite the accurate L-A coupling produced. This is a result of CLM drifting from the initial time of simulation (October 23) towards a solution of considerably colder and drier air with time.

Figure 8 also highlights the impact of the choice of LSM and PBL schemes in the evolution of  $\theta$  and  $q$  over an extended time, including the significant impacts of nocturnal PBL turbulence formulations. There is clearly an underprediction of humidity and a drift towards cooler temperatures from the CLM simulations over the three day period. It is evident from Figs. 7 and 8 that LSM physics dominate the local PBL equilibrium and accuracy of temperature and humidity, but that PBL physics come into play when looking at nocturnal and convective PBL evolution. Once again, the mixing diagram approach, while for the most part limited in focus here to clear-sky daytime conditions, can be used for many conditions and applications (e.g. convection, nocturnal, and long-term studies) that are the subject of ongoing work.

#### 4.1.3 Advection

The mixing diagram theory presented by Betts et al. (1994) also supports inclusion of a horizontal advection vector. As many studies have shown (Kustas and Brutsaert 1987; Peters-Lidard and David 2000; Santanello et al. 2005), one of the main limiting factors (other than entrainment) in closing the heat and moisture budgets of the PBL is advection. Here, advection can be represented by a vector ( $\mathbf{V}_{\text{adv}}$ ) similar

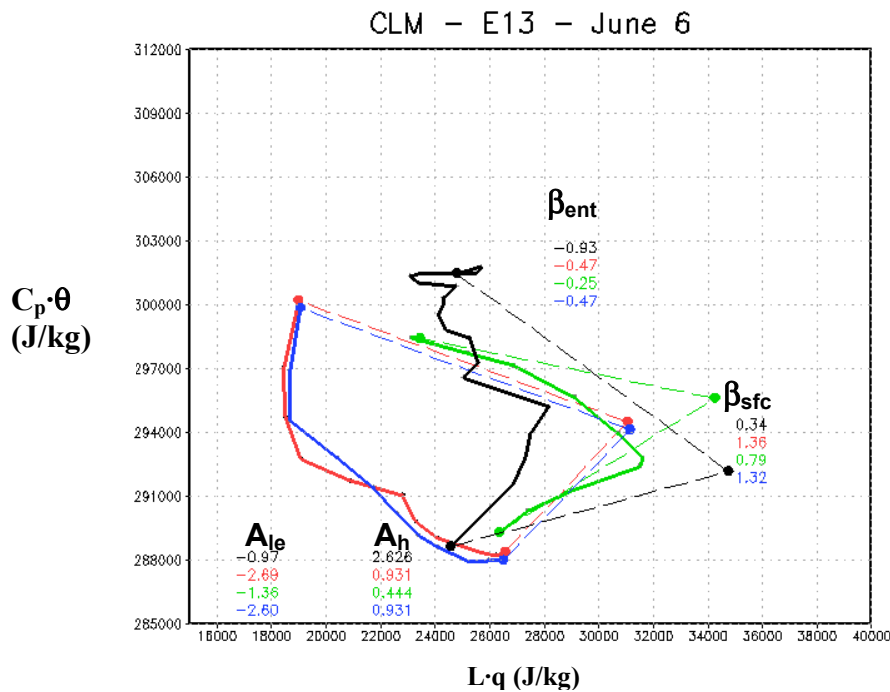
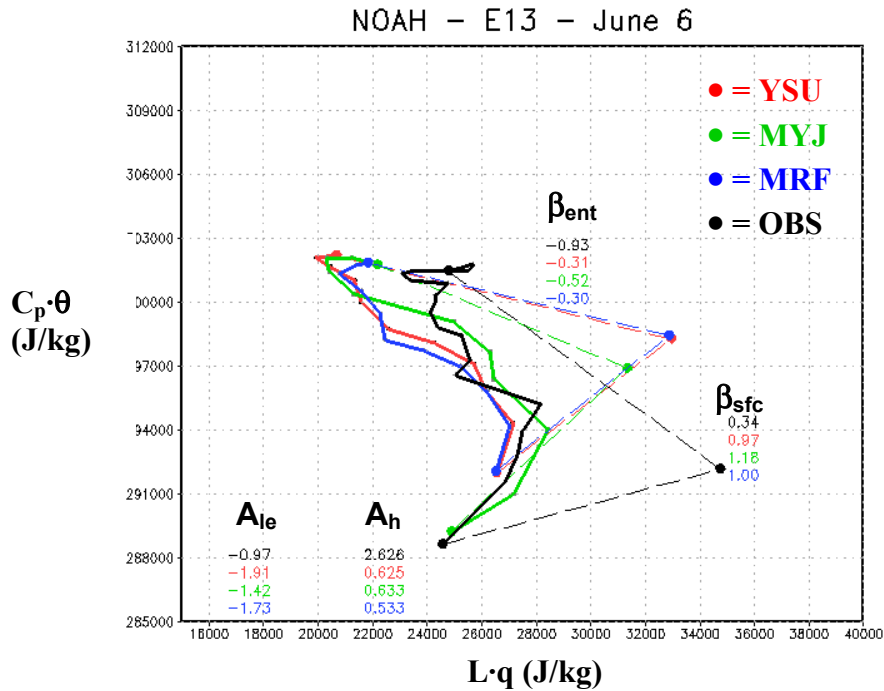


**Figure 6:** Diurnal co-evolution (12-00Z) of 2m-specific humidity ( $Lq$ ) and 2m-potential temperature ( $C_p\theta$ ) on 6 June 2002 as simulated by LIS-WRF for the ARM-SGP CF at Lamont, OK using the a) Noah and b) CLM models and PBL combinations with the associated surface and entrainment vectors and derived metrics. Also overlain are observations from CF and metrics calculated from surface meteorology, flux, and profile measurements (black).

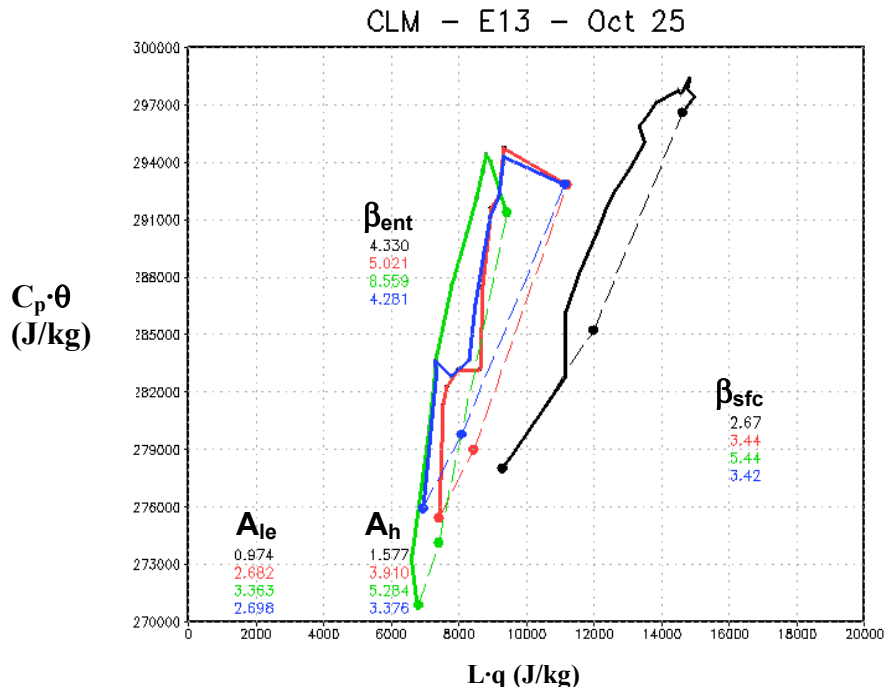
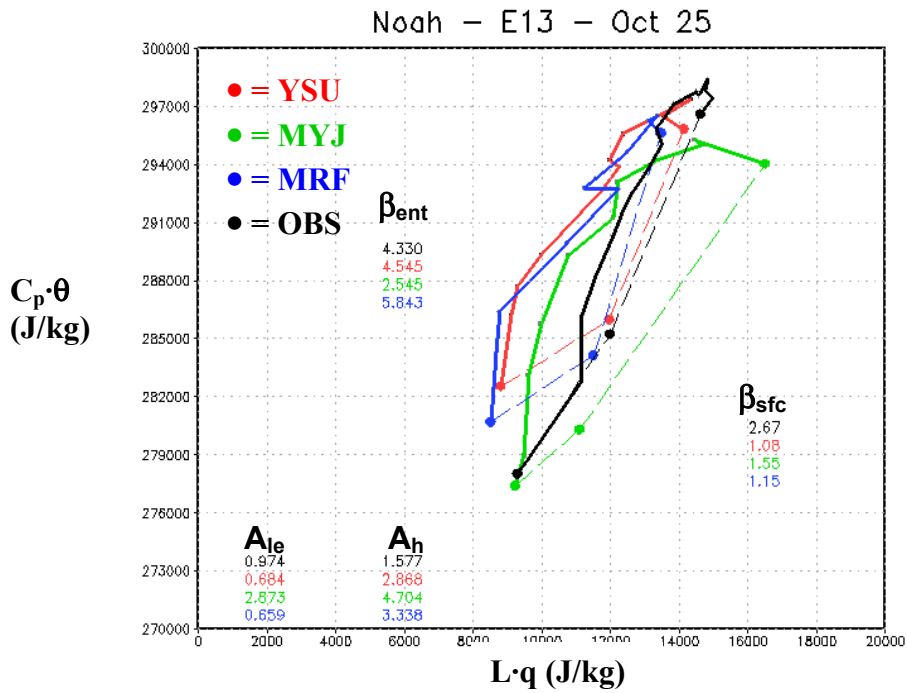
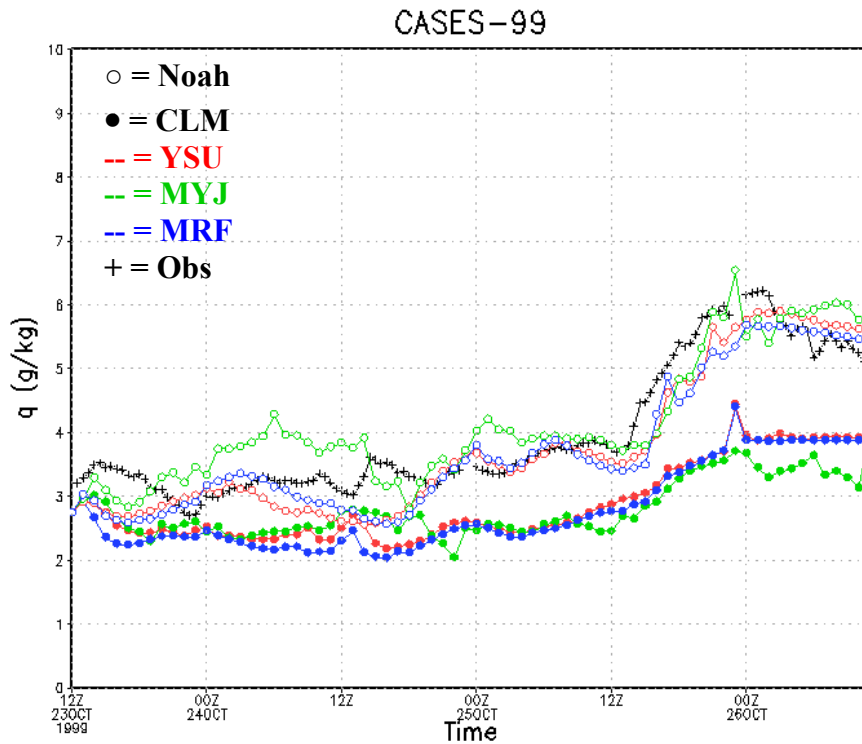
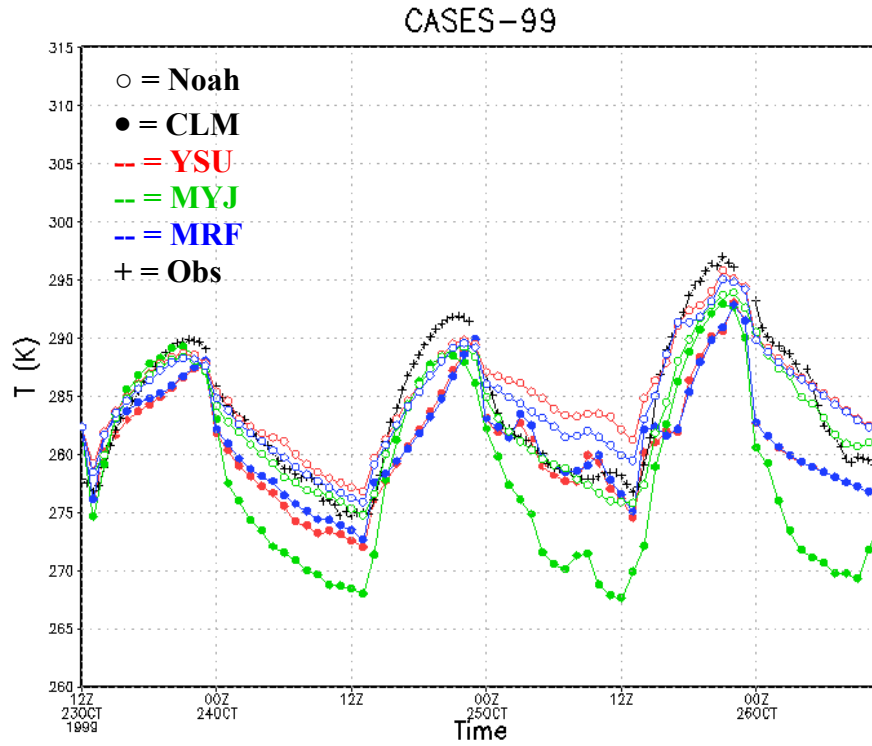


Figure 7: Same as for Figure 6, but for simulations from the CASES-99 experiment at the ARM-SGP CF on 25 October 1999.



**Figure 8:** 2-meter potential temperature ( $T$ ) and specific humidity ( $q$ ) simulated by LIS-WRF over the 72-hour period of the CASES-99 experiment the ARM-SGP CF at Lamont, OK using the a) Noah ( $\circ$ ) and b) CLM ( $\bullet$ ) models coupled to the YSU (red), MYJ (green), and MRF (blue) PBL models combinations with observations at the CF ( $+$ ).

to that of the surface and entrainment fluxes, and represents the horizontal flux of heat and moisture over the 12-hr period. The contribution of advection is calculated and then added to the surface flux vector ( $\mathbf{V}_{adv} + \mathbf{V}_{sfc}$ ), with the new residual representing the entrainment flux (Fig. 9). As such, the surface flux vector is unaffected by the addition of advection, while entrainment clearly is impacted.

Due to the high-resolution of LIS-WRF output (1 km; hourly), it is relatively easy to calculate hourly advection estimates using a finite differencing approach and to regenerate mixing diagrams including all three flux components. As mentioned, there is a peculiar increase in humidity evident in all three simulations in the afternoon. The new diagram indicates that there is, in fact, a significant increase in PBL moisture due to advection throughout the day that supports this humidity increase. It should be noted that advection, while important for this location, was a small vector component of the results presented in Figs. 3-7. However, these results demonstrate that advection can be easily calculated from model output and incorporated into the mixing diagram approach.

#### 4.2 Integrative Diagnostics of LoCo

As shown here, the mixing diagram approach can be used to quantify and evaluate the processes governing the heat and moisture budgets and evolution of the PBL. From a slightly broader perspective, these processes are encapsulated by two observable properties of the system that are reflective of the equilibrium generated by the L-A coupling. First, the forcing from the land surface is best represented by the evaporative fraction ( $EF = LE_{sfc} / (H_{sfc} + LE_{sfc})$ ), which is a function of the flux of heat and moisture from the land to the atmosphere that contributes to the buoyancy and evolution of the PBL.  $EF$  is similar to the Bowen ratio but normalized for incoming available energy, and is typically interchanged with surface moisture availability or soil water content as it controls the surface flux partitioning. The second integrative property that is reflective of local coupling is the maximum PBL height ( $PBLH$ ), as it is a direct function of the L-A interactions (most notably heat and moisture entrainment) controlling PBL growth.

Combined, the relationship between  $EF$  and  $PBLH$  can be thought of as describing the amount of surface forcing generated by a LSM versus what the response of the coupled PBL scheme is relative to those fluxes.

For direct comparison with the results presented earlier, Fig. 10 shows the relationship between  $EF$  and  $PBLH$  generated from LIS-WRF simulations (Noah and CLM) for the dry, intermediate, and wet soil conditions on 12 June 2002. By stratifying over surface moisture regimes, this plot illustrates how different PBL-LSM couplings behave over a wide range of conditions. As was shown in Fig. 3, there is significant PBL growth and dry air entrainment feedback over dry soils that are supported by the low  $EF$  and very high  $PBLH$  seen here. The Noah and CLM simulations with the MYJ PBL showed a slightly different evolution of  $\theta$  and  $q$  and

lower entrainment rates ( $A_h$  and  $A_{le}$ ) than the YSU/MRF schemes, which is reflected in the significantly lower  $PBLH$  reached despite having similar low values of  $EF$  and high surface heating. In this case, the PBL (atmosphere) limits the impact and forcing from the land surface.

For dry and intermediate soil moistures, the CLM simulations produce a slightly lower  $EF$  (higher  $H_{sfc}$ ) than the corresponding Noah runs, but despite this they still reach comparable  $PBLH$  values for each PBL. This is partly due to the CLM spinup initializing a slightly drier soil than Noah for these locations, but also due to the differences in LSM physics controlling evaporation. For wet soils, the reverse is true where  $EF$  is slightly higher in CLM due to slightly higher initial soil water content from the CLM spinup. These features correspond to the differences in  $\mathbf{V}_{sfc}$  between Noah and CLM that was shown in Figs. 3-5.

Overall, these plots depict the sensitivity and accuracy of LSMs and PBL schemes over a range of conditions, and can be similarly examined across vegetation regimes (not shown). There is, as expected, greater sensitivity of  $EF$  to the choice of LSM and moisture regime, while  $PBLH$  varies more significantly between PBL schemes and increasingly so for drier soils when the impacts of the entrainment feedbacks are maximized. It can also be ascertained from these results where the model coupling produces the right answer (e.g.  $PBLH$ ) despite flaws in the representation of specific L-A processes (e.g. surface fluxes, entrainment). This is an important step towards greater and complete understanding and quantification of the components of LoCo.

## 5. DISCUSSION AND CONCLUSIONS

The framework presented here provides a detailed methodology to quantify and evaluate the critical processes controlling local L-A coupling. The results and analyses of the IHOP-02 and CASES-99 experiments were provided as an example of how to apply the mixing diagram approach to model output and observations. While the focus is on diurnal and local scales for convective PBLs, this framework can be easily applied to any coupled model and scales of interest. It is likely that issues such as convection and precipitation will complicate the interpretation of mixing diagrams versus that of a smooth diurnal cycle, but it remains that the full set of governing L-A interactions and processes are still represented and can be valuable. For example, the entrainment Bowen ratio ( $\beta_{ent}$ ) has been shown to be an important determinant of convective initiation, and can be easily derived and evaluated using this approach. These metrics would be valuable to understanding the generation of convection in coupled models by quantifying the L-A processes and feedbacks that are typically difficult to interpret (Trier et al. 2004; Holt et al. 2006)

While the mixing diagram approach is relatively simple, it is important to note that the component vectors and derived metrics are rather sensitive to the mean  $H_{sfc}$ ,  $PBLH$ , and time interval. Mixing diagrams

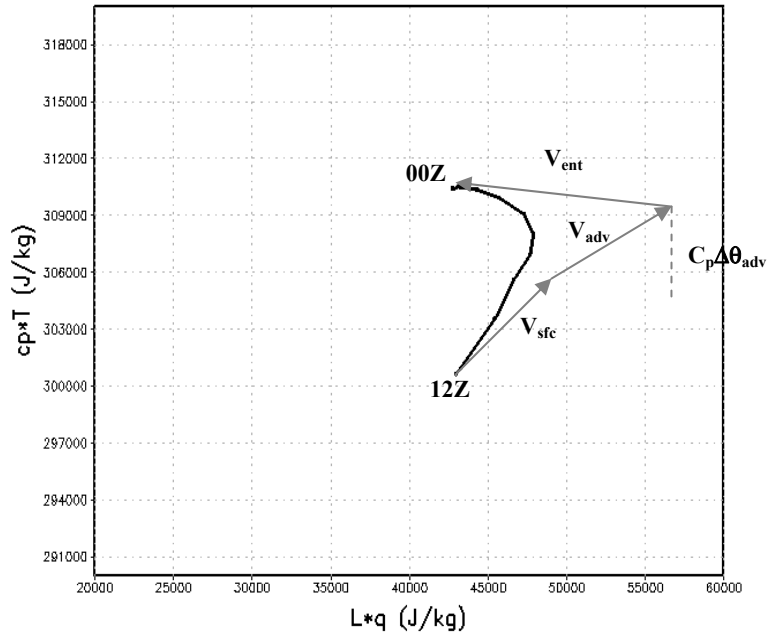


**Figure 9:** Diurnal evolution (12-00Z; solid red line) of 2m-potential temperature ( $C_p \theta$ ) vs. 2m-specific humidity ( $Lq$ ) on 12 June 2002 simulated by LIS-WRF using the Noah LSM with the YSU PBL scheme during the IHOP-02 experiment in the SGP. The annotations on the plots depict the vector component contributions of surface and entrainment fluxes, and the addition of a vector due to the horizontal advection of heat and moisture ( $\mathbf{V}_{adv}$ ).

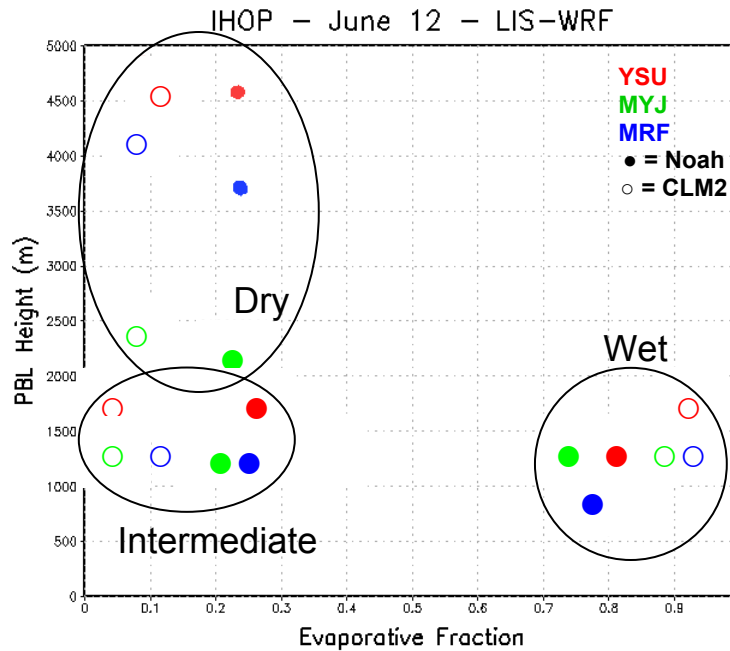


**Figure 10:** Relationship of evaporative fraction ( $LE_{sfc}/(LE_{sfc}+H_{sfc})$ ) to maximum PBL height as simulated by LIS-WRF with the Noah and CLM LSMs at the dry, intermediate, and wet soil locations in Figs. 3-5.

can be generated for as little as a one-hour interval, in which case the time of day becomes critical as it relates to  $H_{sfc}$  and  $PBLH$ . We have performed a preliminary analysis of hourly mixing diagrams and metrics, but for purposes of this study found it less instructive than using the 12-hour daytime interval which is less noisy and integrates the processes responsible for the full PBL evolution. However, it may be possible to look at finer time intervals and develop relationships between surface and entrainment fluxes and their relative dominance throughout the day, and determine if PBL-LSM accuracy is time-dependent as well. Also note that although we included the hourly evolution of  $\theta$  and  $q$  to better illustrate the temporal dynamics at work, only the initial and final values of  $\theta$  and  $q$  are required to obtain the derived metrics.

Ongoing work on advancing the cause of LoCo includes a number of detailed experiments and analyses based on the mixing diagram approach. For example, an evaluation of different methods to spinup Noah and CLM and initialize LIS-WRF is being performed with varying degrees of input forcing and parameter data quality. As mentioned, there were differences in LIS-WRF runs with Noah and CLM due to different initializations from the two model spinups, and it is equally important to evaluate the how different inputs to these models impact the spinups and the LIS-WRF simulations themselves. Therefore, the mixing diagram approach will yield insight into the sensitivity and accuracy of various PBL-LSM couplings to the initial conditions.

Another ongoing experiment is an extended (~7 day) regional LIS-WRF simulation with 2 nested domains covering 6-12 June 2002 during the IHOP-02. This will enable LIS-WRF to evolve over time from synoptically forced, clear-sky conditions with a drydown period ending with the convectively-active 12 June case. As such, there should be a transition seen in the mixing diagrams from each day that reflects the changing surface and atmospheric conditions through the evolution of  $\theta$  and  $q$ . This experiment should also help to extend this approach to longer timescales that are important for seasonal and climate-scale prediction models.

Quantification of L-A interactions is particularly important for land surface data assimilation efforts. While this is a relatively young topic of research, high-quality remote sensing data (e.g. surface temperature, snow, and soil moisture) can be assimilated into LSMs using a variety of techniques. The impacts of the assimilation needs to be understood, however, and are vastly different for offline and coupled tests due to the addition of L-A interactions and feedbacks in the latter. The mixing diagram approach can therefore be an important tool in determining the potential improvement and model sensitivity to assimilation strategies going forward.

Finally, the greater applicability of this methodology to the LoCo community is not limited to modeling studies alone. Recent advances in satellite remote sensing will continue to improve the retrieval of PBL and

land surface data for a number of applications with global coverage and high temporal resolution. This includes the diurnal evolution (due to multiple sensors) of variables such as temperature and humidity (MODIS, AIRS), soil moisture (AMSR, SMOS), evaporation (MODIS, AIRS), and PBL height (AIRS, CALIPSO). As a result, the ability of satellite remote sensing to monitor the PBL and estimate L-A properties and conditions will continue to be improved and can be incorporated to the mixing diagram approach to provide insight into LoCo across the globe.

*Acknowledgements.* This work was supported by the NASA Energy and Water Cycle Study (NEWS) and I would like to thank NEWS, ESSIC, and GSFC for helping to make the completion of this work possible. In particular, Jim Geiger, Charles Alonge, and Joe Eastman were instrumental in providing feedback and activities related to LIS-WRF. We also appreciate the past and ongoing collaboration with the LoCo community that has stimulated this work, in particular Bert Holtslag, Bart van den Hurk, Paul Houser, and Dara Entekhabi.

## 6. References

- Angevine W. M., 1999: Entrainment results including advection and case studies from the Flatland boundary layer experiments. *J. Geophys. Res.*, 104, 30947–30963.
- Anthes, R.A., and T.T. Warner, 1978: Development of Hydrodynamic Models Suitable for Air Pollution and Other Mesometeorological Studies. *Mon. Wea. Rev.*, 106, 1045–1078.
- Barros A. P., and W. Hwu, 2002: A study of land-atmosphere interactions during summertime rainfall using a mesoscale model. *J. Geophys. Res.*, 107, 4227, doi:10.1029/2000JD000254.
- Berbery, E., Y. Luo, K. Mitchell, and A. Betts, 2003: Eta model estimated land surface processes and the hydrological cycle of the Mississippi Basin. *J. Geophys. Res.*, 108, D22, 8852, doi:10.1029/2002JD003192.
- Best, M.J., A. Beljaars, J. Polcher, and P. Viterbo, 2004: A Proposed Structure for Coupling Tiled Surfaces with the Planetary Boundary Layer. *J. Hydrometeorol.*, 5, 1271–1278.
- Betts, A.K., 1984: Boundary Layer Thermodynamics of a High Plains Severe Storm. *Mon. Wea. Rev.*, 112, 2199–2211.
- , 1992: FIFE atmospheric boundary layer budget methods. *J. Geophys. Res.*, 97, 18523–18532.
- , 2000: Idealized model for equilibrium boundary layer over land. *J. Hydrometeorol.*, 1, 507–523.
- , and J. H. Ball, 1994: Budget analysis of FIFE-1987 sonde data. *J. Geophys. Res.*, 99, 3655–3666.
- , and —, 1995: The FIFE surface diurnal cycle climate. *J. Geophys. Res.*, 100, 25674–25693.
- , —, A. C. M. Beljaars, M. J. Miller, and P.A. Viterbo, 1996: The land surface-atmosphere interaction: A review based on observational and global modeling perspectives. *J. Geophys. Res.*, 101, 7209–7226.
- , and P. Viterbo, 2005: Land-surface, boundary layer, and cloud-field coupling over the southwestern Amazon in ERA-40. *J. Geophys. Res.*, 110, D14108, doi:10.1029/2004JD005702.
- Brubaker, K. L., and D. Entekhabi, 1996: Analysis of feedback mechanisms in land-atmosphere interaction. *Water Resour. Res.*, 32, 1343–1357.
- Chen, F., Z. Janic, and K. Mitchell, 1997: Impact of atmospheric-surface layer parameterizations in the new land-surface scheme of the NCEP mesoscale Eta numerical model. *Bound.-Layer Meteorol.*, 85, 391–421.
- Chen, T.H., A. Henderson-Sellers, P.C.D. Milly, A.J. Pitman, A.C.M. Beljaars, J. Polcher, F. Abramopoulos, A. Boone, S. Chang, F. Chen, Y. Dai, C.E. Desborough, R.E. Dickinson, L. Dümenil, M. Ek, J.R. Garratt, N. Gedney, Y.M. Gusev, J. Kim, R. Koster, E.A. Kowalczyk, K. Laval, J. Lean, D. Lettenmaier, X. Liang, J.F. Mahfouf, H.T. Mengelkamp, K. Mitchell, O.N. Nasonova, J. Noilhan, A. Robock, C. Rosenzweig, J. Schaake, C.A. Schlosser, J.P. Schulz, Y. Shao, A.B. Shmakin, D.L. Verseghy, P. Wetzel, E.F. Wood, Y. Xue, Z.L. Yang, and Q. Zeng, 1997: Cabauw Experimental Results from the Project for Intercomparison of Land-Surface Parameterization Schemes. *J. Climate*, 10, 1194–1215.
- Cheng, W.Y.Y., and W.J. Steenburgh, 2005: Evaluation of Surface Sensible Weather Forecasts by the WRF and the Eta Models over the Western United States. *Wea. Forecasting*, 20, 812–821.
- Cleugh H. A., M. R. Raupach, P. R. Briggs, and P. A. Coppin, 2004: Regional-scale heat and water vapour fluxes in an agricultural landscape: An evaluation of CBL budget methods at OASIS. *Bound.-Layer Meteorol.*, 110, 99–137.
- Dai Y. J., Coauthors., 2003: The Common Land Model. *Bull. Amer. Meteor. Soc.*, 84, 1013–1023.
- Desai, A. R., Davis, K. J., Senff, C. J., Ismail, S., Browell, E. V., Stauffer, D. R., and Reen, B. P.: 2006: A Case Study on the Effects of Heterogeneous Soil Moisture on Mesoscale Boundary Layer Structure in the Southern Great Plains, U.S.A. Part I: Simple Prognostic Model. *Bound.-Layer Meteorol.*, 119, DOI: 10.1007/s10546-005-9024-6.
- Diak G. R., 1990: Evaluation of heat flux, moisture flux and aerodynamic roughness at the land surface from knowledge of the PBL height and satellite derived skin temperatures. *Agric. For. Meteorol.*, 22, 505–508.
- Dirmeyer P. A., Z. Guo, and X. Gao, 2004: Comparison, validation, and transferability of eight multiyear global soil wetness products. *J. Hydrometeorol.*, 5, 1011–1033.
- Dolman A., J. Gash, J. Goutorbé, Y. Kerr, T. Lebel, S. Prince, and J. Stricker, 1997: The role of the land surface in Sahelian climate: HAPEX–Sahel results and future research needs. *J. Hydrol.*, 188/189, 1067–1079.
- Ek M. B., and A. A. M. Holtslag, 2004: Influence of soil moisture on boundary layer cloud development. *J. Hydrometeorol.*, 5, 86–99.
- Ek M. B., K. E. Mitchell, Y. Lin, E. Rogers, P. Grunmann, V. Koren, G. Gayno, and J. D. Tarpley, 2003: Implementation of Noah land surface model advances in the National Centers for Environmental Prediction operational mesoscale Eta Model. *J. Geophys. Res.*, 108, 8851, doi:10.1029/2002JD003296.

- Ek, M., and L. Mahrt, 1994: Daytime Evolution of Relative Humidity at the Boundary Layer Top. *Mon. Wea. Rev.*, 122, 2709–2721.
- Eltahir E. A., 1998: A soil moisture–rainfall feedback mechanism: 1. Theory and observations. *Water Resour. Res.*, 34, 765–776.
- Entekhabi, D., and K. L. Brubaker, 1995: An analytic approach to modeling land–atmosphere interaction. 2: Stochastic extension. *Water Resour. Res.*, 31, 633–643.
- Entekhabi D., Coauthors, 1999: An agenda for land surface hydrology research and a call for the second international hydrology decade. *Bull. Amer. Meteor. Soc.*, 80, 2043–2058.
- Findell K. L., and E. A. Eltahir, 2003a: Atmospheric controls on soil moisture–boundary layer interactions: Three-dimensional wind effects. *J. Geophys. Res.*, 108, 8385, doi:10.1029/2001JD001515.
- Findell K. L., and E. A. Eltahir, 2003b: Atmospheric controls on soil moisture–boundary layer interactions. Part I: Framework development. *J. Hydrometeorol.*, 4, 552–569.
- Garratt, J. R., 1992: *The Atmospheric Boundary Layer*. Cambridge University Press, 316 pp..
- Gu, L., T. Meyers, S. G. Pallardy, P. J. Hanson, B. Yang, M. Heuer, K. P. Hosman, J. S. Riggs, D. Sluss, and S. D. Wullschleger (2006), Direct and indirect effects of atmospheric conditions and soil moisture on surface energy partitioning revealed by a prolonged drought at a temperate forest site, *J. Geophys. Res.*, 111, D16102, doi:10.1029/2006JD007161.
- Hacker, J.P., and D. Rostkier-Edelstein, 2007: PBL State Estimation with Surface Observations, a Column Model, and an Ensemble Filter. *Mon. Wea. Rev.*, 135, 2958–2972.
- Hacker, J.P., and C. Snyder, 2005: Ensemble Kalman Filter Assimilation of Fixed Screen-Height Observations in a Parameterized PBL. *Mon. Wea. Rev.*, 133, 3260–3275.
- Henderson-Sellers, A., Z.L. Yang, and R. Dickinson, 1993: The Project for Intercomparison of Land-surface Parameterization Schemes. *Bull. Amer. Meteor. Soc.*, 74, 1335–1349.
- Hess R., 2001: Assimilation of screen-level observations by variational soil moisture. *Meteor. Atmos. Phys.*, 77, 145–154.
- Hogue, T. S., L. Bastidas, H. Gupta, S. Sorooshian, K. Mitchell, and W. Emmerich, 2005: Evaluation and Transferability of the Noah Land Surface Model in Semi-arid Environments. *J. Hydrometeorol.*, 6, 68–84.
- Holt, T. R., D. Niyogi, F. Chen, K. Manning, and M. A. LeMone, and A. Qureshi, 2006: Effect of land-atmosphere interactions on the IHOP 24–25 May 2002 convection case. *Mon. Wea. Rev.*, 134, 113–133.
- Holtlag, A. A. M., G. J. Steeneveld, and B. J. H. van de Wiel, 2007: Role of land-surface temperature feedback on model performance for the stable boundary layer. *Bound.-Layer Meteorol.*, 125, 361–376.
- Hong, S.Y., and H.L. Pan, 1996: Nonlocal Boundary Layer Vertical Diffusion in a Medium-Range Forecast Model. *Mon. Wea. Rev.*, 124, 2322–2339.
- Hong, S.Y., Y. Noh, and J. Dudhia, 2006: A New Vertical Diffusion Package with an Explicit Treatment of Entrainment Processes. *Mon. Wea. Rev.*, 134, 2318–2341.
- Jacobs, C., and H. De Bruin, 1992: The Sensitivity of Regional Transpiration to Land-Surface Characteristics: Significance of Feedback. *J. Climate*, 5, 683–698.
- Janjic, Z. I., 2001: Nonsingular implementation of the Mellor-Yamada level 2.5 scheme in the NCEP meso model. Technical Report 437, National Centers for Environmental Prediction Office.
- Kim C. P., and D. Entekhabi, 1998: Feedbacks in the land-surface and mixed-layer energy budgets. *Bound.-Layer Meteorol.*, 88, 1–21.
- Koster R. D., P. A. Dirmeyer, A. N. Hahmann, R. Ijpeelaar, L. Tyahla, P. Cox, and M. J. Suarez, 2002: Comparing the degree of land–atmosphere interaction in four atmospheric general circulation models. *J. Hydrometeorol.*, 3, 363–375.
- Koster R. D., Coauthors, 2004: Regions of strong coupling between soil moisture and precipitation. *Nature*, 306, 1138–1140.
- Kumar, S. V., C. D. Peters-Lidard, J. L. Eastman, and W.-K. Tao, 2008: An integrated high resolution hydrometeorological modeling testbed using LIS and WRF. *Environmental Modelling and Software*, 23, 169–181.
- Kustas W. P., and W. Brutsaert, 1987: Virtual heat entrainment in the mixed layer over very rough terrain. *Bound.-Layer Meteorol.*, 38, 141–157.
- Lawrence, D.M., and J.M. Slingo, 2005: Weak Land–Atmosphere Coupling Strength in HadAM3: The Role of Soil Moisture Variability. *J. Hydrometeorol.*, 6, 670–680.
- Liu, Y., L. A. Bastidas, H. V. Gupta, and S. Sorooshian, 2003: Impacts of a Parameterization Deficiency on Offline and Coupled Land Surface Model Simulations. *J. Hydrometeorol.*, 4, 901–914.

- Liu, Y., H. V. Gupta, S. Sorooshian, L. A. Bastidas, and W. J. Shuttleworth, 2004: Exploring Parameter Sensitivities of the Land Surface Using a Locally Coupled Land-Atmosphere Model. *J. Geophys. Res.*, 109, 21101-21114.
- Liu, Y., H. V. Gupta, S. Sorooshian, L. A. Bastidas, and W. J. Shuttleworth, 2005: Constraining Land Surface and Atmospheric Parameters of a Locally Coupled Model Using Observational Data. *J. Hydrometeorol.*, 6, 156-172.
- Margulis, S. A., and D. Entekhabi, 2001a: A Coupled Land Surface-Boundary Layer Model and its Adjoint. *J. Hydrometeorol.*, 2, 274-296.
- Margulis, S. A., and D. Entekhabi, 2001b: Feedback between the Land Surface Energy Balance and Atmospheric Boundary Layer Diagnosed through a Model and its Adjoint. *J. Hydrometeorol.*, 2, 599-620.
- Medeiros, B., A. Hall, and B. Stevens, 2005: What Controls the Mean Depth of the PBL? *J. Climate*, 18, 3157-3172.
- Mellor, G. L., and T. Yamada, 1982: Development of a turbulence closure model for geophysical fluid problems. *Rev. Geophys. Space Phys.*, 20, 851-875.
- Michalakes, J., S. Chen, J. Dudhia, L. Hart, J. Klemp, J. Middlecoff, and W. Skamarock, 2001: Development of a next generation regional weather research and forecast model. *Developments in Teracomputing: Proceedings of the Ninth ECMWF Workshop on the use of high performance computing in meteorology*. Singapore, pp. 269-276.
- Molod, A., H. Salmun, and D.W. Waugh, 2004: The Impact on a GCM Climate of an Extended Mosaic Technique for the Land-Atmosphere Coupling. *J. Climate*, 17, 3877-3891.
- Oke T. R., 1987: *Boundary Layer Climates*. 2d ed. Routledge, 435 pp.
- Pan, H.-L., and L. Mahrt, 1987: Interaction between soil hydrology and boundary-layer development. *Bound.-Layer Meteorol.*, 38, 185-202..
- Peters-Lidard C., and L. H. Davis, 2000: Regional flux estimation in a convective boundary layer using a conservation approach. *J. Hydrometeorol.*, 1, 170-182.
- Pitman A. J., Coauthors, 1999: Key results and implications from phase 1(c) of the Project for Intercomparison of Land-surface Parameterization Schemes. *Climate Dyn.*, 15, 673-684.
- Polcher J., Coauthors, 1998: A proposal for a general interface between land-surface schemes and general circulation models. *Global Planet. Change*, 19, 261-276.
- Poulos G. S., Coauthors 2002: CASES-99: A comprehensive investigation of the stable nocturnal boundary layer. *Bull. Amer. Meteor. Soc.*, 83, 555-581.
- Reen, B. P., D. R. Stauffer, K. J. David, and A. Desai, 2006: A Case Study on the Effects of Heterogeneous Soil Moisture on Mesoscale Boundary Layer Structure in the Southern Great Plains, U.S.A. Part II: Mesoscale Modeling. *Bound.-Layer Meteorol.*, 120, DOI: 10.1007/s10546-006-9056-6.
- Rhodin A., F. Kucharski, U. Callies, D. P. Eppel, and W. Wergen, 1999: Variational analysis of effective soil moisture from screen-level atmospheric parameters: Application to a short-range weather forecast model. *Quart. J. Roy. Meteor. Soc.*, 125, 2427-2448.
- Santanello, J. A., M. A. Friedl, and M. Ek: Convective Planetary Boundary Layer Interactions with the Land Surface at Diurnal Time Scales, 2007: Diagnostics and Feedbacks. *J. Hydrometeorol.*, 8, 1082-1097.
- Santanello, J. A., M. A. Friedl, and W. P. Kustas, 2005: Empirical Investigation of Convective Planetary Boundary Layer Evolution and its Relationship with Land Surface Properties and Processes. *J Appl. Meteorol.*, 44, 917-932.
- Seuffert G., H. Wilker, P. Viterbo, M. Drusch, and J. F. Mahfouf, 2004: The usage of screen-level parameters and microwave brightness temperature for soil moisture analysis. *J. Hydrometeorol.*, 5, 516-531. Sorbjan 1995
- Steenefeld, G.J., B.J.H. van de Wiel, and A.A.M. Holtslag, 2006: Modeling the Evolution of the Atmospheric Boundary Layer Coupled to the Land Surface for Three Contrasting Nights in CASES-99. *J. Atmos. Sci.*, 63, 920-935.
- Stull, R. B., 1988: *An Introduction to Boundary Layer Meteorology*. Kluwer Academic, 666 pp..
- Trier, S. B., F. Chen, and K. W. Manning, 2004: A study of convection initiation in a mesoscale model using high-resolution land surface initial conditions. *Mon. Wea. Rev.*, 132, 2954-2976.
- Troen, I., and L. Mahrt, 1986: A simple model of the atmospheric boundary layer: Sensitivity to surface evaporation. *Bound.-Layer Meteorol.*, 37, 129-148..
- van den Hurk, B., A. Holtslag, and C. D. Peters-Lidard, 2005: GLASS and GABLS workshop on local land-atmosphere coupling – 19/21 Sep. 2005: Workshop Summary and LoCo Implementation Plan.
- Weckworth T. M., Coauthors, 2004: An overview of the International H<sub>2</sub>O Project (IHOP\_2002) and some preliminary highlights. *Bull. Amer. Meteor. Soc.*, 85, 253-277.